INORGANIC CHEMISTRY
FRONTIERS

RESEARCH ARTICLE

View Article Online
View Journal | View Issue

Cite this: *Inorg. Chem. Front.*, 2023, **10**, 1270

Catalytic reactions in a Co_{12} cuboctahedral cage arising from guest encapsulation and cage-based redox activation†

Xuejian Zhang, Burin Sudittapong and Michael D. Ward *

A **Co_{12}** coordination cage with a cuboctahedral architecture, and incorporating a mixture of tritopic (face-capping) and ditopic (edge-bridging) ligands, shows strong guest binding of large aromatic fluorophores (fluorescein and its derivatives 6-carboxyfluorescein and Eosin-Y) with 1 : 1 binding constants in water in the range log K = 6.7–7.9; its large central cavity (>1000 Å^3) facilitates binding of much larger guests than was possible with the smaller **Co_8** cage that we have reported previously. Guest binding is accompanied by catalysed reactions of bound guests because the high positive charge on the cage surface (24+) also attracts anions, allowing the organic guests and anionic reaction partners to be co-located, resulting for example in cage-catalysed hydrolysis of phosphate esters (the insecticides Me-paraoxon and Et-paraoxon) and conversion of diacetyl fluorescein to fluorescein. In addition, we demonstrate a new type of cage-based catalysis which relies on the redox activity of the Co(II)/Co(III) couple in the cage to activate the peroxymonosulfate (PMS) anion by converting it to the highly reactive $SO_4^{\bullet-}$ radical ion, which bleaches cavity-bound fluorescein by complete oxidation. This is an example of an 'advanced oxidation process' in which the host cage not only brings the fluorescein and the PMS together *via* orthogonal hydrophobic and electrostatic interactions, but also provides redox activation of the PMS *via* a Co(II)/Co(III) couple, with the cage taking an active role in the catalytic process rather than acting simply as a passive reaction vessel.

Received 19th October 2022,
Accepted 6th January 2023

DOI: 10.1039/d2qi02223k

rsc.li/frontiers-inorganic

Introduction

The enduring interest in the chemistry of self-assembled coordination cages[1] is due in large part to their ability to act as catalysts for chemical transformations of guests bound in their central cavity.[2] Binding of a potential substrate inside a cage cavity can be considered as an approximate model for binding of substrates at enzyme active sites, and the mechanisms by which reactions are accelerated have some obvious similarities between the two cases. Effects responsible for catalysed reactions of substrates bound in cages include conformational changes which bring a flexible substrate close to the conformation of a reaction transition state;[3] electronic effects associated with the high charges which may be carried by multinuclear metal/ligand assemblies;[4] and high local concentrations when two reaction partners are co-located in or around the cage.[5,6]

Our recent work on cage-based catalysis[6] has focussed on our octanuclear cubic $[M_8L_{12}]^{16+}$ system in which a ditopic bis(pyrazolyl-pyridine) bridging ligand spans each of the twelve edges of the assembly of eight M(II) ions which lie at the vertices.[7] The cage has a cavity size (*ca.* 400 Å^3) which is ideal for accommodating a wide range of small organic guests; in its water-soluble forms, the hydrophobic effect ensures strong binding of such guests, with binding constants of up to 10^6 M^{-1} for optimally-sized guests;[6a,b] and the high positive charge allows the cage to accumulate anions around its surface very effectively.[6,8] This last effect is the basis for its catalytic activity as the cage uses two orthogonal[8c] interactions to bring two reaction partners into close proximity, *viz.* (i) an organic substrate which binds in the cage cavity *via* the hydrophobic effect; and (ii) accumulation of anions around the cage surface *via* electrostatic/ion-pairing effects. The result is a high local concentration of ions around a cage-bound guest, leading to catalysed bimolecular reactions such as the Kemp elimination (reaction of benzisoxazole with hydroxide,[6c] or with a basic phenolate anion[6d]), phosphate ester hydrolysis,[6e] or an aldol condensation.[6f]

Whilst this $[Co_8L_{12}]^{16+}$ cubic cage (hereafter abbreviated as **Co_8**) has provided many examples of cage-based catalysis[6] it is of course size- and shape-limited in the guests that it can bind. We were therefore interested to see if we could extend

Department of Chemistry, University of Warwick, Coventry CV4 7AL, UK.
E-mail: m.d.ward@warwick.ac.uk

†Electronic supplementary information (ESI) available: All experimental and characterisation data. See DOI: https://doi.org/10.1039/d2qi02223k

cage-based catalysis to larger members of our coordination cage family which would be able to accommodate a wider range of guests in the central cavity, whilst maintaining the key characteristics that make catalysis possible (a hydrophobic interior cavity surface for organic guest binding; and a high positive charge which attracts anions to the cage surface). This is non-trivial as it requires solubility in water, requiring in some cases significant changes to ligand syntheses to introduce external solubilising substituents such as HO groups[7b] or PEG chains.[7c] Additionally, some of the larger cages that we have prepared exist in solution in slow equilibria between larger cages and smaller assemblies which prevents meaningful analysis of host/guest chemistry.[9]

In this paper we introduce the cuboctahedral cage **Co_{12}** (Fig. 1) as a catalyst for reactions between hydrophobic substrates and anions in water, using a range of ester hydrolysis reactions as illustrations. Significantly, we also report extension of the range of cage-catalysed reactions to include some that require not just co-location of reaction partners around the cage, but redox activation of one of the reagents by the Co (II) ions in the cage. This is an additional degree of sophistication in the cage-based catalysed reactions, making the cage not just an inert container that holds components in close proximity to one another, but also an active participant in electron-transfer steps required for the catalytic cycle in a way that has been demonstrated in recent examples of photo-redox catalysis.[10] This additional redox-based participation of the cage in catalytic processes will substantially extend the scope of reaction types that can be catalysed.

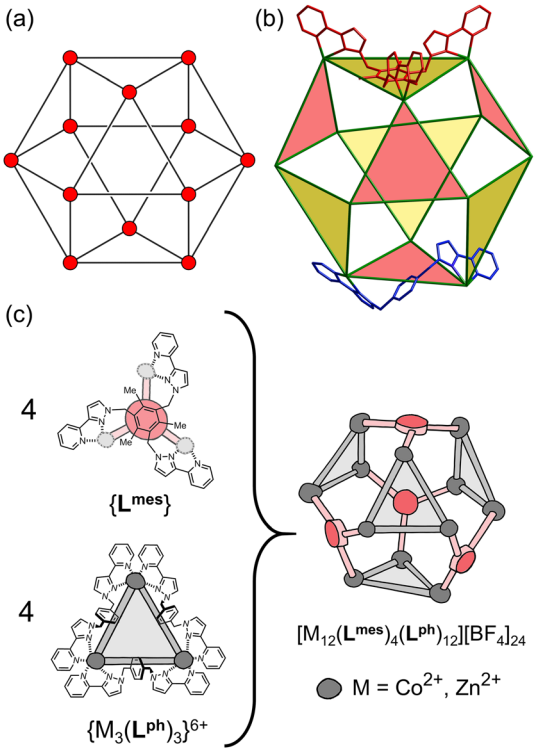

Fig. 1 (a) An idealised cuboctahedron; (b) partial crystal structure of $[Cu_{12}(L^{ph})_{12}(L^{mes})_4](BF_4)_{24}$ (taken from ref. 11*a*) emphasising the cuboctahedral M_{12} core with the four triangular faces capped by tritopic ligands L^{mes} coloured yellow, and the alternate four triangular faces – which are $Cu_3(\mu\text{-}L^{ph})_3$ cyclic helicates – coloured pink; (c) additional sketch emphasising the disposition of the four $M_3(\mu\text{-}L^{ph})_3$ cyclic helicate faces in these structures (grey triangles) and the four L^{mes} ligands which connect them (red). Figure reproduced with modifications from ref. 11*b*.

Results and discussion

The Co_{12} cage and its water solubilisation

As the candidate for extending our cage-based catalysis studies we have chosen the M_{12} cuboctahedral cage shown in Fig. 1.[11] This is based on a mixture of two different types of ligand (edge-bridging, ditopic, L^{ph}; and face-capping, tritopic, L^{mes}). A combination of four equivalents of L^{mes} and twelve equivalents of L^{ph} combine with twelve M(II) ions to form a cuboctahedral array $[M_{12}(L^{ph})_{12}(L^{mes})_4]^{24+}$ in which four of the eight M_3 triangular faces are capped by an L^{mes} ligand, and the other four are edge-bridged, forming a set of (chiral) $M_3(L^{ph})_3$ cyclic helicates.[11*a*] Interestingly the four triangular cyclic helicate faces can vary their sense of helicity between 'anticlockwise' (A) and 'clockwise' (C) independently of one another, which means that the $[M_{12}(L^{ph})_{12}(L^{mes})_4]^{24+}$ cage can exist as a mixture of three different diastereoisomers: (i) all four cyclic helicate faces homochiral (enantiomeric pair AAAA/CCCC, T symmetry); (ii) three cyclic helicate faces of one chirality and one of the other (enantiomeric pair AAAC/CCCA, C_3 symmetry); and finally (iii) two cyclic helicates of each chirality (AACC, S_4 symmetry, which has no enantiomer).[11*b*] The result is a set of three M_{12} cages of essentially the same size and with very similar arrangement of metal ions at the vertices, differing only in the chiralities of the cyclic helicate faces. Examples of all three diastereoisomers of this type of cuboctahedral cage have been individually structurally characterised in previous work.[11*b*] Separation of the three diastereoisomers in significant quantities beyond picking individual crystals was not possible given their essentially identical size/shape and identical charge. Importantly for the purposes of this work, the cavity volumes of the three diastereoisomers are very similar to one another (1036–1121 Å^3)[11*b*] and substantially larger than the cavity of the M_8L_{12} cubic cage (409 Å^3)[6] so we expect fundamentally different host/guest chemistry. For the purposes of this work, therefore, the set of three similar diastereoisomers of the $[Co_{12}(L^{ph})_{12}(L^{mes})_4]^{24+}$ cage is considered as a single species.

Initially therefore we combined $Co(BF_4)_2$, L^{ph} and L^{mes} in a 12 : 12 : 4 ratio in the previously-reported way[11] to obtain solid $[Co_{12}(L^{ph})_{12}(L^{mes})_4](BF_4)_{24}$ (hereafter abbreviated as **Co_{12}**). High-resolution ES mass spectrometry confirmed formation of the cage with a characteristic sequence of signals associated with loss of different numbers of anions giving the species $\{[Co_{12}(L^{ph})_{12}(L^{mes})_4](BF_4)_{24-n}\}^{n+}$ (n = 4–9, Fig. S1–S4;† with the correct fractional isotope spacings and isotopic patters in the high-resolution signals). In the ^{1}H NMR spectrum in CD_3CN (Fig. S5†), the paramagnetism associated with use of high-spin

Co(II) ions acts as a convenient shift reagent, spreading out the signals over a 200 ppm chemical shift range.[7a] The spectrum is clearly highly complex due to the mixture of three diastereoisomers with different symmetries and cannot be assigned in detail: but we can identify in some parts of the spectrum a characteristic set of eight signals (subsets of 1, 3 and 4 signals with the same intensity within each subset)‡ which arise from one chemical type of proton (*e.g.* a pyridyl H^6 from L^{mes}) in the three diastereoisomers, as described earlier.[11b] In the ^{1}H NMR spectrum for **Co_{12}** in MeCN we can identify exactly this pattern between −10 and −23 ppm (Fig. S5,† top panel) which, together with the mass spectrum, confirms formation of **Co_{12}** with all three diastereoisomers present.

The complex formed beautiful crystals on recrystallisation from a variety of solvents which however failed to diffract X-rays significantly, even using synchrotron radiation, which is likely a consequence of co-crystallisation of the three diastereoisomers which will lead to extensive disorder in the organic ligand positions and (to a lesser extent) in the metal atom positions. Indeed the NMR spectrum of redissolved apparently 'single' crystals matched that of the bulk as-prepared material, showing the mixture of diastereoisomers to be present in the crystals. We note however that several other crystal structures of this M_{12} cage family have been previously reported.[11]

For control experiment purposes we also prepared the isostructural **Zn_{12}** cage in exactly the same way; this complex too was characterised by high-resolution ES mass spectrometry (Fig. S7–S10†), showing the sequence $\{[Zn_{12}(L^{ph})_{12}(L^{mes})_4](BF_4)_{24-n}\}^{n+}$ (n = 4–9) with the expected isotope patterns and spacings for the individual species. The ^{1}H NMR spectrum of **Zn_{12}** (Fig. S11†) is mostly unassignable due to the overlap of signals in the aromatic region associated with the mixture of diastereoisomers, but in the aliphatic region we can clearly see the singlets for the methyl protons of L^{mes}: a set of four of the same intensity for the S_4 isomer and a set of three of the same intensity for the C_3 isomer. We cannot see the additional signal arising from the T isomer (expected between 0 and 1 ppm)[11b] so we conclude that the **Zn_{12}** complex consists of the S_4 and C_3 isomers: in the previously-reported **Cd_{12}** species, the T isomer was by far the least abundant of the three.[11b] A DOSY spectrum (Fig. S12†) confirms that a single species (ignoring the isomerism) is present in solution, and from the diffusion coefficient [$\log(D/m^2\ s^{-1}) = -9.8$] we can estimate from the Stokes–Einstein equation that the radius of the complex is *ca.* 12 Å, which is close to the crystallographically-observed average radius of *ca.* 14 Å and far larger than any species such as individual ligands or low-nuclearity complexes.

Having confirmed formation of **Co_{12}** (and **Zn_{12}** for control experiments) the next problem is water-solubilisation to allow the hydrophobic effect to be exploited for guest binding. Appending hydroxymethyl or PEG substituents to the ligands is possible but laborious,[7b,c] and we found that ligand substituents in the obvious positions (pyridyl C^4) caused steric problems which prevented cage assembly – a problem which did not arise earlier in the M_8L_{12} cube where the pyridyl C^4 substituents do not clash.[7b] We have also used anion metathesis, with the usual fluoroborate anions associated with the cage synthesis being replaced by chloride ions which rendered the $[M_8L_{12}]^{16+}$ cage highly water soluble.[6d] However similar anion-exchange experiments to convert **Co_{12}** to its chloride salt did not lead to sufficiently high water solubility and also results in partial decomposition, possibly because chloride is a good competing ligand for Co(II) and the high positive charge on this cage will result in a high chloride ion concentration around the cage following anion metathesis.

We found however that we could successfully water-solubilise **Co_{12}** for catalysis in two different ways which did not require anion-exchange or complex synthetic chemistry associated with incorporation of ligand substituents. These are (i) inclusion of 1% dmso in the aqueous solvent;[6g] and (ii) more unusually, use of a non-ionic surfactant. Use of a small amount of dmso in the aqueous solvent (dmso/water 1 : 99, v/v) provided sufficient solubility for many spectroscopic and catalysis measurements with **Co_{12}** as we report below.§ The non-ionic surfactant polysorbate-20 (also known as Tween-20) also proved to be effective. Tween-20 contains a water-soluble branched poly-oxyethylene terminus functionalised with a lauryl ester chain which provides a hydrophobic terminus. As such one of the applications of Tween-20 is to render water-soluble a range of hydrophobic species, including drug molecules for formulation purposes[12] and hydrophobic membrane proteins during extraction following cell lysis,[13] and it turned out to be very effective at allowing **Co_{12}** to be water-solubilised to a surprisingly high (mM range) concentration. Addition of solid **Co_{12}** to commercial Tween-20, followed by overnight stirring, sonication, dilution with water, and filtration through a 2-micron filter afforded a clear aqueous solution whose con-

‡In the T-symmetry isomer all such protons are equivalent, giving a single signal for all twelve of them. In the C_3-symmetry isomer there are four inequivalent environments (with equal likelihood) for each proton, and in the S_4-symmetry isomer there are three inequivalent environments (with equal likelihood) for each such proton. The result is a set of eight signals, being sets of 1 + 3 + 4 for the three diastereoisomers, and if the assembly of the four triangular helicate faces in the cuboctahedron is purely statistical with no preference for any one diastereoisomer, all eight signals should be of equal intensity (see ref. 11*b*). Any bias towards one diastereoisomer and away from the others will result in a very characteristic set of closely-spaced 1 + 3 + 4 signals for each chemical environment of proton.

§We could also achieve significant water solubility using 10% MeCN in water, a solvent mixture that allowed greater solubility than 1% dmso in water, and we used 10% MeCN in water for some of the NMR and MS experiments to confirm stability of the cages in water. Notably this gave cleaner ES mass spectra than did 1% dmso in water, as the presence of dmso results in greater fragmentation and adduct formation at the high temperatures required for solvent evaporation under MS conditions (compare Fig. S1/S3, and S7/S9†). For the catalysis experiments however we used either Tween-20 or 1% dmso in water to achieve water solubility, to maximise the amount of water present and hence the hydrophobic effect responsible for guest binding. We note that a small admixture of dmso to facilitate water solubility has not caused any stability problems with other members of this cage family based on Co(II) tris(pyrazolyl-pyridine) metal complex units, see for example ref. 6*g*.

centration was established by UV/Vis spectroscopy. A dynamic light scattering experiment (Fig. S14†) confirmed formation of particles with an average size of 12 nm, associated with formation of the Tween-20 micelles which contain **Co_{12}** inside their hydrophobic interiors: we denote the Tween-encapsulated cage molecules as **TW20⊂Co_{12}**. ^{1}H NMR spectra of the resulting solutions were uninformative due to the large excess of Tween present, and the slow tumbling of **Co_{12}** molecules in the micellar environment which broadened the spectra beyond the normal effects of paramagnetism: however the UV/Vis spectrum in the presence of Tween/water was the same as in MeCN/water (10/90).

Guest binding in Co_{12} in water

Initial studies on guest binding focussed on the set of four of guests shown in Scheme 1: these are fluorescein (**FLU**), 6-carboxyfluorescein (**6FLU**), Eosin-Y (**EY**) and hydroxypyrene-trisulfonate (**HPTS**). All of these are fluorescent so we could monitor guest uptake into **Co_{12}** by following fluorescence quenching as portions of **TW20⊂Co_{12}** were added to a fixed concentration (1 μM) of the potential guest in aqueous solution. Binding is clearly strong (Fig. 2): fitting the curve for quenching of **FLU** (a dianion under the prevailing conditions) for example, to a 1 : 1 binding isotherm, afforded a log K value of 6.7. A Job plot based on the fluorescence titration data confirmed 1 : 1 binding, and an electrospray mass spectrum of a **Co_{12}/FLU** mixture showed a set of strong signals associated with the 1 : 1 **Co_{12}·FLU** adduct associated with varying numbers of anions (Fig. S13†). This behaviour is notably different from what we observed for the interaction of **FLU** with the smaller **Co_8** cage, which is too small to accommodate **FLU** inside the cavity: in that case external surface binding occurred with up to five **FLU** units interacting with the **Co_8** cage exterior according to the Job plot, and a much smaller binding constant.[8b] In contrast, with **Co_{12}** as the host, we are clearly seeing (a) much stronger binding of fluorescein and (b) this binding is in a 1 : 1 ratio as shown by both a Job plot and an electrospray mass spectrum, all of which is consistent with cavity-based binding of the single **FLU** guest.

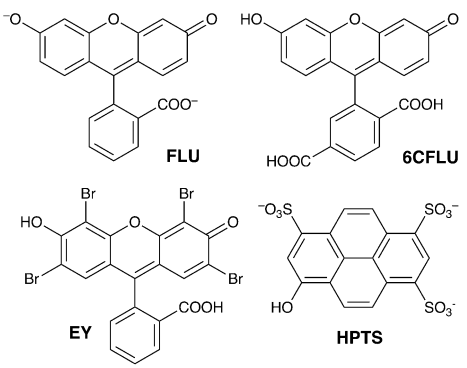

Scheme 1 The aromatic, anionic fluorophores used in this work (shown in the forms that exist in weakly acidic solution).

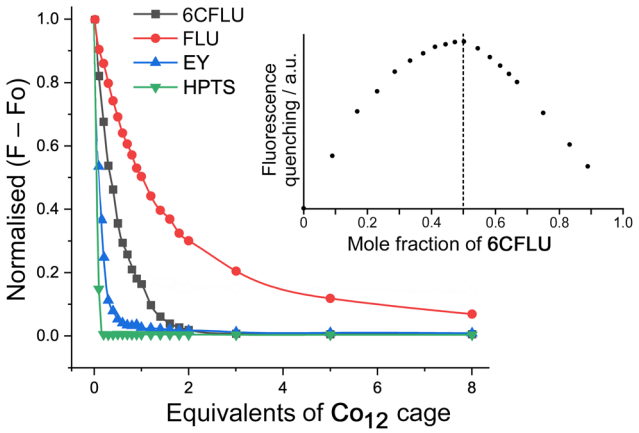

Fig. 2 Fluorescence titrations performed by adding **Co_{12}** (up to 8 equivalents) to a range of different fluorescent dyes (1 μM in water, pH 7, no buffer) showing progressive fluorescence quenching of the dyes as they bind in the **Co_{12}** cavity; the resulting 1 : 1 binding constants are in the main text. A Job plot confirming 1 : 1 binding for guest **6CFLU** is shown in the inset; exactly similar Job plots were obtained with **FLU** and **EY**.

The binding constant (log K = 6.7) with **FLU** is already much larger than we have observed with virtually all other cage/guest complexes using **Co_8**,[6a] which can be ascribed to a combination of (i) the higher hydrophobic surface area of fluorescein compared to the smaller guests that can fit inside the **Co_8** cage, and (ii) an electrostatic contribution associated with the 2− charge on fluorescein and the 24+ charge on **Co_{12}**. We found no evidence for further association of larger numbers of **FLU** guests associated with external surface binding which could still in principle be possible: if it does occur, it is clearly much weaker than the cavity binding.

The related guests **6CFLU** and **EY** bind even more strongly (log K values of 7.0 and 7.9 respectively, with 1 : 1 **Co_{12}** : guest binding according to Job plots – see Fig. 2, inset, for an example), which we ascribe to the higher negative charge (of **6CFLU**, 3−) and higher hydrophobicity (of **EY**) respectively, compared to **FLU**.[8b] **HPTS** – a trianion – binds too strongly for a binding constant to be determined under these conditions but clearly behaves differently: the very rapid quenching (≪1 equivalent of **Co_{12}** is needed to completely quench the HPTS fluorescence) implies that binding is not just cavity-based but there is also a surface interaction whereby one **Co_{12}** binds and quenches multiple equivalents of HPTS around its exterior, in a manner analogous to the **Co_8/FLU** system.[8b]

Co_{12}-catalysed phosphotriester hydrolysis

To examine the ability of **TW20⊂Co_{12}** to act as a catalyst using the same mechanism as we observed with the cubic **Co_8** cage (co-location of hydrophobic substrate and anions using orthogonal interactions)[6e] we examined the catalysed hydrolysis of the phosphotriesters methyl- and ethyl-paraoxon (4-$O_2NC_6H_4O$–P(=O)$(OR)_2$, with R = Me or Et respectively), which are potent acetylcholinesterase-inhibiting insecticides,

and contain 4-nitrophenolate as the leaving group from the hydrolysis reaction, allowing facile monitoring of hydrolysis reaction rates by UV/Vis spectroscopy.

Under a range of catalyst and substrate concentration conditions (using fixed pH 8, borate buffer, see Fig. 3 and S16†) we obtained second-order rate constants for the cage-catalysed hydrolysis of these paraoxons of *ca.* 0.5 M^{-1} s^{-1} for methyl-paraoxon and 0.4 M^{-1} s^{-1} for ethyl-paraoxon which are 1–2 orders of magnitude faster than we observed using **Co_8** as the catalyst under similar conditions.[6e] Exactly similar behaviour (with slightly smaller rate accelerations) was observed using 1% dmso in water as the solvent rather than the aqueous Tween-20 surfactant (see ESI†).

In our earlier work using **Co_8** we found that the cage-catalysed hydrolysis of methyl-paraoxon occurred at the external surface of the cage, as the substrate did not bind in the **Co_8** cavity for steric reasons. Nonetheless the hydrophobicity of the *exterior* surface allowed methyl-paraoxon to associate with it in aqueous solution, and the 16+ charge on the cage attracted hydroxide ions, so the cage surface still served as a medium to attract and co-locate the two reaction partners around the exterior surface, even if the resulting catalysis did not benefit from the substrate lying inside the cavity. With **TW20⊂Co_{12}** as the catalyst the much (2.5×) larger cage cavity will allow methyl- and ethyl-paraoxon to bind inside it, surrounded by hydroxide ions that are also attracted by the 24+ surface charge, resulting in the catalysed hydrolysis of both substrates that we observe at a rate higher than was previously observed for an external surface-based reaction. From these observations we can expect that the larger cavity of **Co_{12}** will facilitate catalysed reactions of hydrophobic cavity-binding guests with anions with a much wider range of substrates compared to **Co_8**.

Co_{12}-catalysed carboxylate ester hydrolysis

Another illustration of a cage-catalysed reaction involving an ester substrate and hydroxide ions as the reaction partner is provided by the hydrolysis of diacetyl fluorescein (DAF; see Scheme 2) to fluorescein which can be readily followed by monitoring the grow-in of the absorption band for the fluorescein dianion as the reaction proceeds.[6g]

Under conditions where DAF shows no significant hydrolysis over several hours (0.25 mM DAF, 50 mM PBS buffer at pH 7) the presence of **Co_{12}** results in appearance of the fluorescein absorption band at a rate which increases linearly with **Co_{12}** concentration (Fig. 4): dividing the initial rate constant by the **Co_{12}** concentration gives a second order rate constant for the cage-catalysed hydrolysis of DAF of 0.24 M^{-1} s^{-1}. This is between one and two orders of magnitude greater than the catalysis of DAF hydrolysis by the smaller cage **Co_8** under similar conditions:[6g] in that case DAF cannot bind inside the cavity and the reaction occurs at the external surface of the cage with the substrate held by hydrophobic interactions in the hydroxide-rich region around the cationic surface. With **Co_{12}** in contrast the improvement in catalytic rate enhancement compared to **Co_8** implies that DAF is binding inside the cage cavity, surrounded by the layer of surface-bound hydroxide ions, and we have observed before how encapsulation of guests can result in much higher catalysed reaction rates.[6c]

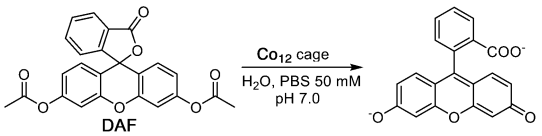

Scheme 2 Hydrolysis of diacetyl fluorescein.

Co_{12}-catalysed oxidation of dyes using peroxymonosulfate: an 'advanced oxidation process' involving cage-based redox activation

We demonstrate here a quite different example of a cage-catalysed reaction which requires not only the co-location of two reaction partners [the dye fluorescein, and the powerful anionic oxidant peroxy-monosulfate (PMS)] but also participation of the Co(II) ions in the cage in a redox cycle. PMS is of great interest as a powerful oxidant for destroying toxins and organic impurities as part of waste-water treatment where it

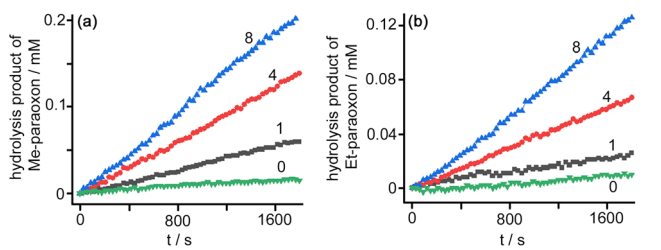

Fig. 3 Catalysed hydrolysis (pH 8, 298 K) of the phosphate esters (a) Me-paraoxon (0.45 mM) and (b) Et-paraoxon (0.49 mM) monitored by UV/Vis absorbance of the accumulating 4-nitrophenolate ion at 400 nm. The green, black, red and blue traces correspond to addition of 0, 1, 4 and 8 mol% of **Co_{12}** (used as the **TW20⊂Co_{12}** solution).

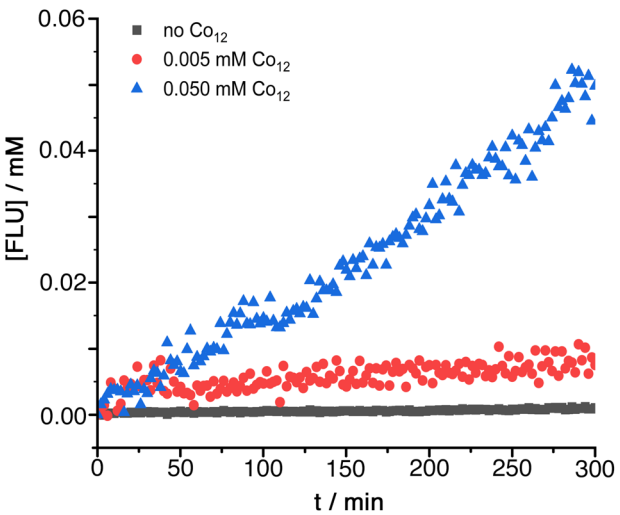

Fig. 4 Catalysed hydrolysis of DAF by **Co_{12}** in 99 : 1 water/dmso at the indicated catalyst concentrations: 0.25 mM DAF, 50 mM PBS buffer, pH 7, 298 K.

has emerged as a desirable alternative to H_2O_2 and other sources of more conventional 'reactive oxygen species' such as $^1O_2$ and $HO^{\bullet}$ in so-called 'advanced oxidation processes'.[14] Importantly, despite its strong thermodynamic oxidising ability, direct reaction of PMS with the contaminants that it is intended to destroy is kinetically slow, and in practice PMS requires activation by any of a wide range of methods that cleaves the peroxide O–O bond to generate the $SO_4^{\bullet-}$ sulfate radical anion which is the species that is predominantly responsible for rapid oxidation of organic contaminants in water, ultimately to innocuous CO_2 and H_2O.[14]

A common method to activate PMS is a redox reaction with a low oxidation state metal ion, with Co(II) being reportedly particularly effective,[14b] according to eqn (1).

$$Co^{2+} + HSO_5^- \rightarrow Co^{3+} + SO_4^{\bullet-} + HO^- \quad (1)$$

Given that $\mathbf{Co_{12}}$ can encapsulate fluorescein in the cavity, and the high positive charge of $\mathbf{Co_{12}}$ means that it should also have the ability to accumulate anions in the same way as $\mathbf{Co_8}$ does (as the ester hydrolysis catalytic studies reported above confirm), we can expect that fluorescein and PMS will be co-located in and around molecules of $\mathbf{Co_{12}}$. In addition, the Co(II) ions in the cage can, if necessary, provide the necessary activation of PMS *via* a Co(II)/Co(III) couple, with the resulting $SO_4^{\bullet-}$ again being held close to the $\mathbf{Co_{12}}$ cage (and its encapsulated substrate) by the 24+ charge on the cage.

In the absence of $\mathbf{TW20{\subset}Co_{12}}$, an aqueous solution of fluorescein (7.5 μM) also containing 45 equivalents of PMS showed no significant degradation of fluorescein as shown by the invariance of its UV/Vis absorption spectrum over time. In the presence of 10 mol% of $\mathbf{Co_{12}}$ however the fluorescein absorption at 490 nm was quickly bleached (Fig. 5, red trace; Fig. S17†), disappearing completely within half an hour (97% loss in 20 minutes) with a pseudo-first-order rate constant of 0.0016 s^{-1} under the prevailing conditions. Effects of different concentrations of $\mathbf{Co_{12}}$ are shown in Fig. S18.† Varying the concentration of added PMS (between 15 and 60 equivalents compared to $\mathbf{Co_{12}}$ catalyst) made little difference, and we speculate that this is because the high affinity of anions for the 24+ cage surface means that the surface becomes quickly saturated with the anions such that addition of more makes no difference. We observed the same non-intuitive effect with the Kemp elimination of cavity-bound benzisoxazole using the $\mathbf{Co_8}$ catalyst: HO^- ions accumulate around the cage surface sufficiently strongly even at pH ≈ 8 that the cage surface becomes saturated, and increasing the pH makes no further difference to the local concentration of hydroxide ions around the guest.[6c] Consequently the reaction rate was invariant in $[HO^-]$ over a considerable pH range despite the mechanism implying that the reaction should be first order in $[HO^-]$.[6c]

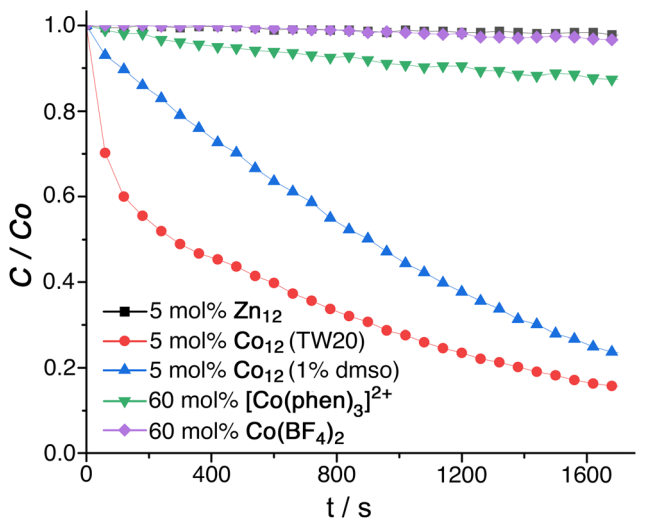

Fig. 5 Destruction of fluorescein by oxidation with peroxo-monosulfate under different sets of conditions, showing the importance of *both* cage-based encapsulation (red and blue lines *vs.* green and purple) and the importance of having Co(II) ions in the cage superstructure as redox agents for activation of peroxymonosulfate (red *vs.* black lines).

Similar results were obtained with the dyes rhodamine and methylene blue, with 5 mol% of $\mathbf{TW20{\subset}Co_{12}}$ resulting in 98% degradation of rhodamine after 20 minutes and 90% degradation of methylene blue after 3 minutes. We note that this type of PMS-based oxidative degradation has not been reported before with fluorescein, and it will be facilitated by the relative ease of oxidation of fluorescein compared to the other organic materials present in the cage superstructure.[15]

We observed that addition of 0.2 M *t*-butanol to the catalytic system – a known scavenger of hydroxyl radicals, but not of $SO_4^{\bullet-}$ radicals[16] – did not change the reaction rate. In contrast addition of 0.2 M MeOH, which can scavenge *both* hydroxyl and $SO_4^{\bullet-}$ radicals,[17] reduced the rate of degradation of fluorescein and resulted in only *ca.* 75% bleaching by the end of the experiment. This sensitivity of the reaction to MeOH, but not to *t*-BuOH, confirms that $SO_4^{\bullet-}$ radicals (but not hydroxyl radicals) are involved, which in turn confirms that redox activation of PMS by Co(II) ions is required before the reaction can occur.

Thus, $\mathbf{Co_{12}}$ in water could in principle accelerate the destruction of fluorescein by PMS in two ways. Firstly, co-location of the two reaction partners, either inside the cage cavity or around its exterior surface, could provide the catalysis following the example provided by the Kemp elimination and other reactions catalysed by $\mathbf{Co_8}$.[6] Secondly the presence of Co(II) ions in the cage provides redox activation of the PMS by converting it to the more reactive species $SO_4^{\bullet-}$ according to eqn (1).[14b] Some control experiments clarify these issues.

Firstly, replacement of $\mathbf{Co_{12}}$ as catalyst by the isostructural cuboctahedral cage $\mathbf{Zn_{12}}$, whilst keeping all other conditions the same, completely stopped the degradation of fluorescein (Fig. 5, black trace). Co-location of fluorescein and PMS in and around the $\mathbf{M_{12}}$ cage cavity alone is an insufficient condition for catalysis: the redox-based activation of the PMS to generate $SO_4^{\bullet-}$ is also required, as the quenching experiments with MeOH/*t*-BuOH showed. Use of $Co(BF_4)_2$ as activator was ineffective, with a mixture of fluorescein/PMS/$Co(BF_4)_2$ showing no degradation of fluorescein (Fig. 5, purple trace). However the Co^{2+}/Co^{3+} couple in water is highly positive – around +1.8 V –

meaning that aqueous Co^{2+} ions are poor reducing agents: a better comparison is with a Co(II) complex in an N_6 coordination environment similar to that which occurs in this cage family, with a much lower redox potential, that would make it a more effective activation agent for PMS according to eqn (1).

Accordingly the final control experiment was to investigate bleaching of fluorescein in a mixture of fluorescein/PMS/[Co(phen)$_3$]$^{2+}$ (phen = 1,10-phenanthroline)[18] in which the N_6-coordinated Co(II) ions are present at the same total concentration as in **Co$_{12}$**, *i.e.* the concentration of mononuclear [Co(phen)$_3$]$^{2+}$ is 12 times the molar concentration that was used for **Co$_{12}$**. The [Co(phen)$_3$]$^{2+/3+}$ redox potential has been reported as +0.62 V *vs.* NHE (−0.02 V *vs.* ferrocene/ferrocenium, Fc/Fc$^+$)[18a] and in a separate paper as −0.04 V *vs.* Fc/Fc$^+$.[18b] This is much less positive than for $Co(BF_4)_2$, and is also lower than the Co^{2+}/Co^{3+} couple of **Co$_{12}$** for which we observed an electrochemically irreversible oxidation (presumably due to a forbidden spin-state change associated with the Co^{2+}/Co^{3+} interconversion) at +0.62 V *vs.* Fc/Fc$^+$ in MeCN (Fig. S19†), making [Co(phen)$_3$]$^{2+}$ an even better reducing agent for activation of PMS than is **Co$_{12}$**. Despite this, in the presence of [Co(phen)$_3$]$^{2+}$ but in the absence of **Co$_{12}$** (*i.e.* with redox activation of PMS available, but without cage-based encapsulation of components) we observed only slow degradation of fluorescein, to the extent of about 10% reduction in absorbance after half an hour (Fig. 5, green trace): this is far slower than was observed in the presence of **Co$_{12}$**.

These experiments confirm that the effective oxidative destruction of fluorescein using **Co$_{12}$** as catalyst arises from a combination of three factors. These are the ability of **Co$_{12}$** to (i) bind fluorescein strongly in water inside its cavity; (ii) accumulate anionic reaction partners around its positively-charged surface, bringing PMS anions close to the fluorescein substrate; and (iii) provide redox activation of the PMS using the Co(II) ions in the cage superstructure which facilitate its conversion to reactive $SO_4^{\bullet-}$ radicals. Removal of *either* the redox activation provided by the Co(II) ions in the cage (control experiment using **Zn$_{12}$**) *or* the cage-based co-encapsulation of reactants (control experiment using [Co(phen)$_3$]$^{2+}$ for activation) stops the effective oxidation catalysis provided by **Co$_{12}$**/PMS system. Finally we note that using the alternative method of water-solubilisation of **Co$_{12}$** (addition of 1% dmso as co-solvent) also provided a clear catalysis of the fluorescein oxidation reaction by PMS (Fig. 5, blue trace) although the effect is less strong than when using Tween-20, an observation which mirrors what we observed (above) for cage-catalysed phospho-ester hydrolysis when the water/Tween-20 reaction medium afforded slightly better catalysis than water/dmso (99 : 1).

Conclusions

In conclusion we have demonstrated that the **Co$_{12}$** cage can be solubilised in water (either using a neutral surfactant or by inclusion of 1% dmso in the solvent), permitting a range of guest binding and reactivity studies that rely on the hydrophobic effect. In aqueous solution **Co$_{12}$** binds a range of organic fluorophores (fluorescein and analogues) very strongly ($K \approx 10^7$ M^{-1}) in the central cavity. The ability of the **Co$_{12}$** cage to co-locate hydrophobic organic substrates and anions using two orthogonal interactions results in catalysed hydrolysis destruction of two phosphate-ester based insecticides and also of diacetyl fluorescein which incorporates two carboxylic ester groups. In both cases the second order rate constants for the catalysed reactions are significantly (1–2 orders of magnitude) larger than we previously observed using the smaller cage **Co$_8$**, which is suggestive of cavity-based catalysis in the larger cavity of **Co$_{12}$** compared to exterior surface-based catalysis using **Co$_8$**.

In addition, **Co$_{12}$** exhibits a new type of cage-catalysed reaction, specifically the destruction of fluorescein by PMS as a model for the 'advanced oxidation process' reactions that are studied to remove organic pollutants from water using peroxymonosulfate. This involves not just the ability of the **Co$_{12}$** cage to bring the organic substrate and the anionic reaction partners into close proximity, but also requires redox activation of PMS (initial conversion to $SO_4^{\bullet-}$ radicals) using the Co(II) ions in the cage – which is therefore an active redox partner in the reaction as well as acting to co-locate the substrates in and around the cage cavity. This type of direct participation of redox-active ions in the cage superstructure in catalysed reactions, which means that the cage is no longer just acting as an inert reaction vessel, offers substantial promise for use of the cages in redox- and photo-redox catalysis processes.

Author contributions

X. Z.: cage synthesis, guest binding and catalysis studies, data analysis. B. S.: NMR and MS studies. M. D. W.: project supervision and manuscript preparation.

Conflicts of interest

There are no conflicts to declare.

Acknowledgements

We thank (i) the University of Warwick (UK) for financial support *via* a Warwick/Monash Alliance accelerator grant involving X. Z.; and (ii) the Development and Promotion of Science and Technology Talents Project, Thailand, for a PhD studentship to B. S.

References

1 (*a*) T. R. Cook and P. J. Stang, Recent Developments in the Preparation and Chemistry of Metallacycles and Metallacages via Coordination, *Chem. Rev.*, 2015, **115**, 7001; (*b*) T. R. Cook, Y.-R. Zheng and P. J. Stang, Metal–Organic Frameworks and Self-Assembled Supramolecular

Coordination Complexes: Comparing and Contrasting the Design, Synthesis, and Functionality of Metal–Organic Materials, *Chem. Rev.*, 2013, **113**, 734; (*c*) R. Chakrabarty, P. S. Mukherjee and P. J. Stang, Supramolecular Coordination: Self-Assembly of Finite Two- and Three-Dimensional Ensembles, *Chem. Rev.*, 2011, **111**, 6810; (*d*) M. M. J. Smulders, I. A. Riddell, C. Browne and J. R. Nitschke, Building on architectural principles for three-dimensional metallosupramolecular construction, *Chem. Soc. Rev.*, 2013, **42**, 1728; (*e*) D. Zhang, T. K. Ronson and J. R. Nitschke, Functional Capsules via Subcomponent Self-Assembly, *Acc. Chem. Res.*, 2018, **51**, 2423; (*f*) H. Vardhan, M. Yusubov and F. Verpoort, Self-assembled metal-organic polyhedra: An overview of various applications, *Coord. Chem. Rev.*, 2016, **306**, 171; (*g*) E. G. Percástegui, T. K. Ronson and J. R. Nitschke, Design and Applications of Water-Soluble Coordination Cages, *Chem. Rev.*, 2020, **120**, 13480.

2 (*a*) Y. Fang, J. A. Powell, E. Li, Q. Wang, Z. Perry, A. Kirchon, X. Yang, Z. Xiao, C. Zhu, L. Zhang, F. Huang and H.-C. Zhou, Catalytic reactions within the cavity of coordination cages, *Chem. Soc. Rev.*, 2019, **48**, 4707; (*b*) C. J. Brown, F. D. Toste, R. G. Bergman and K. N. Raymond, Supramolecular catalysis in metal-ligand cluster hosts, *Chem. Rev.*, 2015, **115**, 3012; (*c*) M. Yoshizawa, J. K. Klosterman and M. Fujita, Functional Molecular Flasks: New Properties and Reactions within Discrete, Self-Assembled Hosts, *Angew. Chem., Int. Ed.*, 2009, **48**, 3418; (*d*) M. Otte, Size-Selective Molecular Flasks, *ACS Catal.*, 2016, **6**, 6491; (*e*) C. M. Hong, R. G. Bergman, K. N. Raymond and F. D. Toste, Self-Assembled Tetrahedral Hosts as Supramolecular Catalysts, *Acc. Chem. Res.*, 2018, **51**, 2447; (*f*) W.-X. Gao, H.-N. Zhang and G.-X. Jin, Supramolecular catalysis based on discrete heterometallic coordination-driven metallacycles and metallacages, *Coord. Chem. Rev.*, 2019, **386**, 69; (*g*) M. Morimoto, S. M. Bierschenk, K. T. Xia, R. G. Bergman, K. N. Raymond and F. D. Toste, Advances in supramolecular host-mediated reactivity, *Nat. Catal.*, 2020, **3**, 969.

3 (*a*) D. M. Kaphan, F. D. Toste, R. G. Bergman and K. N. Raymond, Enabling New Modes of Reactivity via Constrictive Binding in a Supramolecular-Assembly-Catalyzed Aza-Prins Cyclization, *J. Am. Chem. Soc.*, 2015, **137**, 9202; (*b*) C. J. Hastings, M. D. Pluth, R. G. Bergman and K. N. Raymond, Enzymelike Catalysis of the Nazarov Cyclization by Supramolecular Encapsulation, *J. Am. Chem. Soc.*, 2010, **132**, 6938.

4 (*a*) M. D. Pluth, R. G. Bergman and K. H. Raymond, Acid catalysis in basic solution: a supramolecular host promotes orthoformate hydrolysis, *Science*, 2007, **316**, 85; (*b*) M. D. Pluth, R. G. Bergman and K. N. Raymond, Proton-Mediated Chemistry and Catalysis in a Self-Assembled Supramolecular Host, *Acc. Chem. Res.*, 2009, **42**, 1650; (*c*) J. Wang, T. A. Young, F. Duarte and P. J. Lusby, Synergistic Noncovalent Catalysis Facilitates Base-Free Michael Addition, *J. Am. Chem. Soc.*, 2020, **142**, 17743; (*d*) C. M. Hong, M. Morimoto, E. A. Kapustin, N. Alzakhem, R. G. Bergman, K. N. Raymond and F. D. Toste, Deconvoluting the Role of Charge in a Supramolecular Catalyst, *J. Am. Chem. Soc.*, 2018, **140**, 6591.

5 (*a*) J. Kang and J. Rebek Jr., Acceleration of a Diels–Alder reaction by a self-assembled molecular capsule, *Nature*, 1997, **385**, 50; (*b*) M. Yoshizawa, M. Tamura and M. Fujita, Diels-alder in aqueous molecular hosts: unusual regioselectivity and efficient catalysis, *Science*, 2006, **312**, 251; (*c*) Y. Nishioka, T. Yamaguchi, M. Yoshizawa and M. Fujita, Unusual [2+4] and [2+2] Cycloadditions of Arenes in the Confined Cavity of Self-Assembled Cages, *J. Am. Chem. Soc.*, 2007, **129**, 7000; (*d*) S. Horiuchi, T. Murase and M. Fujita, Diels–Alder Reactions of Inert Aromatic Compounds within a Self-Assembled Coordination Cage, *Chem. – Asian J.*, 2011, **6**, 1839.

6 (*a*) M. D. Ward, C. A. Hunter and N. H. Williams, Coordination Cages Based on Bis(pyrazolylpyridine) Ligands: Structures, Dynamic Behavior, Guest Binding, and Catalysis, *Acc. Chem. Res.*, 2018, **51**, 2073; (*b*) M. D. Ward, C. A. Hunter and N. H. Williams, Guest Binding and Catalysis in the Cavity of a Cubic Coordination Cage, *Chem. Lett.*, 2017, **46**, 2; (*c*) W. Cullen, M. C. Misuraca, C. A. Hunter, N. H. Williams and M. D. Ward, Highly efficient catalysis of the Kemp elimination in the cavity of a cubic coordination cage, *Nat. Chem.*, 2016, **8**, 231; (*d*) W. Cullen, A. J. Metherell, A. B. Wragg, C. G. P. Taylor, N. H. Williams and M. D. Ward, Catalysis in a Cationic Coordination Cage Using a Cavity-Bound Guest and Surface-Bound Anions: Inhibition, Activation, and Autocatalysis, *J. Am. Chem. Soc.*, 2018, **140**, 2821; (*e*) C. G. P. Taylor, A. J. Metherell, S. P. Argent, F. M. Ashour, N. H. Williams and M. D. Ward, Coordination-Cage-Catalysed Hydrolysis of Organophosphates: Cavity- or Surface-Based?, *Chem. – Eur. J.*, 2020, **26**, 3065; (*f*) C. Mozaceanu, C. G. P. Taylor, J. R. Piper, S. P. Argent and M. D. Ward, Catalysis of an Aldol Condensation Using a Coordination Cage, *Chemistry*, 2020, **2**, 22; (*g*) A. B. Solea, B. Sudittapong, C. G. P. Taylor and M. D. Ward, Inside or outside the box? Effect of substrate location on coordination-cage based catalysis, *Dalton Trans.*, 2022, **51**, 11277.

7 (*a*) I. S. Tidmarsh, T. B. Faust, H. Adams, L. P. Harding, L. Russo, W. Clegg and M. D. Ward, Octanuclear cubic coordination cages, *J. Am. Chem. Soc.*, 2008, **130**, 15167; (*b*) M. Whitehead, S. Turega, A. Stephenson, C. A. Hunter and M. D. Ward, Quantification of solvent effects on molecular recognition in polyhedral coordination cage hosts, *Chem. Sci.*, 2013, **4**, 2744; (*c*) G. D. Jackson, M. B. Tipping, C. Pritchard, C. G. P. Taylor, J. R. Piper, C. Mozaceanu and M. D. Ward, A Family of Externally-Functionalised Coordination Cages, *Chemistry*, 2021, **3**, 1203.

8 (*a*) M. D. Ludden, C. G. P. Taylor, M. B. Tipping, J. S. Train, N. H. Williams, J. C. Dorrat, K. L. Tuck and M. D. Ward, Interaction of anions with the surface of a coordination

cage in aqueous solution probed by their effect on a cage-catalysed Kemp elimination, *Chem. Sci.*, 2021, **12**, 14781; (*b*) M. D. Ludden and M. D. Ward, Outside the box: quantifying interactions of anions with the exterior surface of a cationic coordination cage, *Dalton Trans.*, 2021, **50**, 2782; (*c*) M. D. Ludden, C. G. P. Taylor and M. D. Ward, Orthogonal binding and displacement of different guest types using a coordination cage host with cavity-based and surface-based binding sites, *Chem. Sci.*, 2021, **12**, 12640.

9 (*a*) W. Cullen, C. A. Hunter and M. D. Ward, An Interconverting Family of Coordination Cages and a *meso*-Helicate; Effects of Temperature, Concentration, and Solvent on the Product Distribution of a Self-Assembly Process, *Inorg. Chem.*, 2015, **54**, 2626; (*b*) A. Stephenson, S. P. Argent, T. Riis-Johannessen, I. S. Tidmarsh and M. D. Ward, Structures and Dynamic Behavior of Large Polyhedral Coordination Cages: An Unusual Cage-to-Cage Interconversion, *J. Am. Chem. Soc.*, 2011, **133**, 858.

10 (*a*) X. Jing, C. He, Y. Yang and C. Duan, A Metal–Organic Tetrahedron as a Redox Vehicle to Encapsulate Organic Dyes for Photocatalytic Proton Reduction, *J. Am. Chem. Soc.*, 2015, **137**, 3967; (*b*) L. Yang, X. Jing, C. He, Z. Chang and C. Duan, Redox-Active M_8L_6 Cubic Hosts with Tetraphenylethylene Faces Encapsulate Organic Dyes for Light-Driven H_2 Production, *Chem. – Eur. J.*, 2016, **22**, 18107.

11 (*a*) N. K. Al-Rasbi, I. S. Tidmarsh, S. P. Argent, H. Adams, L. P. Harding and M. D. Ward, Mixed-Ligand Molecular Paneling: Dodecanuclear Cuboctahedral Coordination Cages Based on a Combination of Edge-Bridging and Face-Capping Ligands, *J. Am. Chem. Soc.*, 2008, **130**, 11641; (*b*) S. P. Argent, F. C. Jackson, H. M. Chan, S. Meyrick, C. G. P. Taylor, T. K. Ronson, J. P. Rourke and M. D. Ward, A family of diastereomeric dodecanuclear coordination cages based on inversion of chirality of individual triangular cyclic helicate faces, *Chem. Sci.*, 2020, **11**, 10167.

12 (*a*) P. Saveyn, E. Cocquyt, W. Zhu, D. Sinnaeve, K. Haustraete, J. C. Martins and P. Van der Meeren, Solubilization of flurbiprofen within non-ionic Tween 20 surfactant micelles: a ^{19}F and ^{1}H NMR study, *Phys. Chem. Chem. Phys.*, 2009, **11**, 5462; (*b*) K. Hoppe and M. Sznitowska, The Effect of Polysorbate 20 on Solubility and Stability of Candesartan Cilexetil in Dissolution Media, *AAPS PharmSciTech*, 2014, **15**, 1116; (*c*) J. Akbari, M. Saeedi, K. Morteza-Semnani, H. R. Kelidari, F. S. Moghanlou, G. Zareh and S. Rostamkalaei, The Effect of Tween 20, 60, and 80 on Dissolution Behavior of Sprionolactone in Solid Dispersions Prepared by PEG 6000, *Adv. Pharm. Bull.*, 2015, **5**, 435.

13 (*a*) S. Hjertén and K.-E. Johansson, Selective solubilization with Tween 20 of membrane proteins from *Acholeplasma laidlawii*, *Biochim. Biophys. Acta*, 1972, **288**, 312; (*b*) L. Liljas, P. Lundahl and S. Hjertén, The major sialoglycoprotein of the human erythrocyte membrane. Release with a non-ionic detergent and purification, *Biochim. Biophys. Acta*, 1974, **352**, 327; (*c*) S. Schuck, M. Honsho, K. Ekroos and K. Simons, Resistance of cell memebranes to different detergents, *Proc. Natl. Acad. Sci. U. S. A.*, 2003, **100**, 5795; (*d*) V. Kotov, K. Bartels, K. Veith, I. Josts, U. K. T. Subhramanyam, C. Günther, J. Labahn, T. C. Marlovits, I. Moraes, H. Tidow, C. Löw and M. Garcia-Alai, High-throughput stability screening for detergent-solubilized membrane proteins, *Sci. Rep.*, 2019, **9**, 10379.

14 (*a*) J. Wang and S. Wang, Activation of persulfate (PS) and peroxymonosulfate (PMS) and application for the degradation of emerging contaminants, *Chem. Eng. J.*, 2018, **334**, 1502; (*b*) F. Ghanbari and M. Moradi, Application of peroxymonosulfate and its activation methods for degradation of environmental organic pollutants: Review, *Chem. Eng. J.*, 2017, **310**, 41; (*c*) X. Zheng, X. Niu, D. Zhang, M. Lv, X. Ye, J. Ma, Z. Lin and M. Fu, Metal-based catalysts for persulfate and peroxymonosulfate activation in heterogeneous ways: A review, *Chem. Eng. J.*, 2022, **429**, 132323; (*d*) J. Lee, U. von Gunten and J.-H. Kim, Persulfate-Based Advanced Oxidation: Critical Assessment of Opportunities and Roadblocks, *Environ. Sci. Technol.*, 2020, **54**, 3064.

15 (*a*) N. L. Queiroz, J. A. M. Nascimento, M. L. Nascimento, V. B. Nascimento and S. C. B. Oliveira, Oxidation Mechanism of Fluorescein at Glassy Carbon Electrode, *Electroanalysis*, 2017, **29**, 489; (*b*) O. K. Lebedeva, V. S. Snytko, I. I. Kuznetsova, D. Y. Kultin, A. N. Zakharov and L. M. Kustov, Unusual Behavior of Fluorescein under Conditions of Electrochemical Oxidation in an Aqueous Phosphate Buffer Solution, *Russ. J. Phys. Chem.*, 2019, **93**, 168; (*c*) S. Pirillo, F. S. G. Einschlag, M. L. Ferreira and E. H. Rueda, Eriochrome Blue Black R and Fluorescein degradation by hydrogen peroxide oxidation with horseradish peroxidase and hematin as biocatalysts, *J. Mol. Catal. B: Enzym.*, 2010, **66**, 63.

16 M. Piechowski, M. A. Thelen, J. Hoigné and R. E. Bühler, tert-Butanol as an OH-Scavenger in the Pulse Radiolysis of Oxygenated Aqueous Systems, *Ber. Bunsenges. Phys. Chem.*, 1992, **96**, 1448.

17 R. Li, J. Kong, H. Liu, P. Chen, G. Liu, F. Li and W. Lv, A sulfate radical based ferrous–peroxydisulfate oxidative system for indomethacin degradation in aqueous solutions, *RSC Adv.*, 2017, **7**, 22802.

18 (*a*) S. M. Feldt, G. Wang, G. Boschloo and A. Hagfeldt, Effects of Driving Forces for Recombination and Regeneration on the Photovoltaic Performance of Dye-Sensitized Solar Cells using Cobalt Polypyridine Redox Couples, *J. Phys. Chem. C*, 2011, **115**, 21500; (*b*) H. Ferreira, M. M. Conradie and J. Conradie, Electrochemical properties of a series of Co(II) complexes containing substituted phenanthrolines, *Electrochim. Acta*, 2018, **292**, 489.

